Wavelength-Dependent Collagen Fragmentation during Mid-IR Laser Ablation

Yaowu Xiao,* Mingsheng Guo,[†] Kevin Parker,[‡] and M. Shane Hutson*

*Department of Physics & Astronomy and Vanderbilt Institute for Integrative Biosystem Research & Education, Vanderbilt University, Nashville, Tennessee; [†]Department of Physics, Fisk University, Nashville, Tennessee; and [‡]Department of Physics, Duke University, Durham, North Carolina

ABSTRACT   Mid-infrared free-electron lasers have proven adept in surgical applications. When tuned to wavelengths between 6 and 7 μm, such lasers remove defined volumes of soft tissue with very little collateral damage. Previous attempts to explain the wavelength-dependence of collateral damage have invoked a wavelength-dependent loss of protein structural integrity. However, the molecular nature of this structural failure has been heretofore ill-defined. In this report, we evaluate several candidates for the relevant transition by analyzing the nonvolatile debris ejected during ablation. Porcine corneas were ablated with a free-electron laser tuned to 2.77 or 6.45 μm—wavelengths with matched absorption coefficients for hydrated corneas that respectively target either tissue water or protein. The debris ejected during these ablations was characterized via gel electrophoresis, as well as Fourier transform infrared spectroscopy, micro-Raman and ^{13}C-NMR spectroscopy. We find that high-fluence (240 J/cm^2) ablation at 6.45 μm, but not at 2.77 μm, leads to protein fragmentation accompanied by the accumulation of nitrile and alkyne species. The candidate transition most consistent with these observations is scission of the collagen protein backbone at N-alkylamide bonds. Identifying this transition is a key step toward understanding the observed wavelength-dependence of collateral damage in mid-infrared laser ablation.

INTRODUCTION

The two-pronged goal of laser surgery is to remove a defined target-volume of tissue while minimally affecting adjacent tissue. One demonstrated way to achieve this goal is with pulsed mid-infrared (IR) lasers, particularly those that target ubiquitous tissue chromophores like water or protein. Regardless of the targeted chromophore, tissue removal with mid-IR lasers is driven by the explosive vaporization of water (1). Expansion of this vaporized water is constrained; and tissue removal ultimately depends on a structural failure of the protein matrix.

To minimize collateral damage to the surrounding tissue, material removal must commence before absorbed energy diffuses out of the target volume, i.e., the pulse must be thermally-confined (2). However, thermal confinement by itself is not sufficient. Experiments with tunable mid-IR lasers have shown that at very high fluence (several hundred times the ablation threshold), there is an additional mid-IR wavelength-dependence—less collateral damage is observed at wavelengths where the predominant chromophore is protein (3). Edwards and co-workers hypothesized that direct absorption by protein could lead to a less violent removal of tissue (and thus less collateral damage) through a pre-vaporization loss of protein structural integrity; however, this structural failure has not been well defined. In this study, we present detailed spectroscopic (Fourier transform infrared (FTIR), Raman, and ^{13}C-NMR) and electrophoretic evidence that the relevant structural failure is scission of the protein backbone at N-alkylamide bonds (N-C$_\alpha$). The accumulation of backbone scissions is much greater at high fluences and at wavelengths that directly target protein instead of water.

In this analysis, we ablate porcine corneas and use a CaF$_2$ window in a catcher foil setup to collect the ejected, nonvolatile tissue droplets. Although a surgeon would consider this material as ablation debris, its characterization elucidates the protein chemistry relevant to ablation. Previous investigations have collected the plumes generated during ArF excimer and Er:YAG laser ablation, but only analyzed the gaseous fraction (4). Very little of the ablated protein (molecular weights of order 100 kDa) is actually converted into such small volatile species (40–400 Da). This investigation is more similar to that of Auerhammer and co-workers who ablated corneas with the tunable output of a mid-IR free-electron laser (FEL) and measured the size distribution of the ejected droplets. Even when the ablating wavelengths were well-matched (in terms of cornea's overall absorption coefficient), the ejected droplets were much smaller for wavelengths that directly targeted protein (5). In the experiments presented here, we have ablated porcine corneas using a similar FEL, but tuned to a different pair of matched wavelengths: 6.45 μm that targets the amide II vibration of proteins; and 2.77 μm that targets the OH stretch of water.

MATERIALS AND METHODS

Sample preparation

Corneas were obtained from sacrificed pig eyes within 24 h post-mortem, and the epithelial layer was removed with an ethanol-soaked swab. The

corneas were washed with distilled water to remove any contaminant on the surface, and then pressed between two pieces of soft paper to absorb excess surface water. For each tissue sample, a strip of cornea and sclera ($\sim 25 \times 5$ mm) was affixed to a metal substrate with cyanoacrylate glue applied to the scleral regions at the far ends of the strip. Normal hydration of the corneas was maintained by periodically squirting saline onto the surface and blotting off the excess. For some experiments, samples were allowed to dehydrate at room temperature for 2–3 h until they had lost 30% of their original mass, i.e., a 40% decrease in hydration. Control samples from porcine corneas were prepared by drying thin slices ($\sim 5 \mu$m) of stroma taken from samples frozen at $-20°$C. Purified collagen was obtained from a limited pepsin A digestion of porcine corneas (6).

Laser parameters

The Vanderbilt Mark-III FEL has a complex pulse structure in which 3–5 μs long macropulses are delivered at 1–30 Hz (7). Each macropulse is composed of a micropulse train in which the 1–3 ps long micropulses occur at a repetition rate of 2.85 GHz.

To collect ablation debris, the central region of an excised strip of cornea was irradiated by the FEL through a CaF_2 window that captured the debris as it was ejected. All ablations and debris collections were performed in an air atmosphere. The gap between window and cornea surfaces was ~ 0.5 mm and the FEL spot diameter at the sample surface (measured with a knife edge) was 100–200 μm. The sample and window were moved together to typically collect debris from 30–40 ablation spots (at 1.0 mm intervals) per sample/window pair. Typical exposure parameters for the experiments described here were 5–10 macropulses at ~ 20 mJ per macropulse; however, samples for micro-Raman analysis were ablated in only one spot with a single macropulse. With these conditions, macropulse fluences of 60 or 240 J/cm^2 were attained. Note that all references to fluence in this report correspond to macropulse fluence.

FTIR spectroscopy

The ablation debris was vacuum-dried onto the CaF_2 windows used for collection and then used directly for FTIR spectroscopy. For control samples, the slice thickness was selected so that the amide I absorbance was between 0.1–0.2. Spectra were measured in an evacuated Bruker FTIR spectrometer (IFS-66v) with a typical average of 128 scans and a spectral resolution of 4 cm^{-1}.

Micro-Raman spectroscopy

Spectra were recorded on a commercial Raman microspectrometer (LabRam, Jobin-Yvon), using a grating of 1800 grooves/mm and a He-Ne laser (632.8 nm) at 11 mW. A silicon wafer was used for wavelength calibration. Ablation debris was collected as before; however, ablation at each spot was limited to a single pulse. Micro-Raman spectra were recorded of the debris in situ on the CaF_2 window surface from 4-μm diameter spots at several sites within the debris field. At each site, five 100-s acquisitions were averaged to increase signal/noise ratio. The five spectra from each site were reproducible, indicating no accumulation of damage due to He-Ne irradiation.

^{13}C-NMR spectroscopy

To obtain enough material for NMR analysis, we pooled the debris collected on ~ 200 CaF_2 windows for a single exposure condition (6.45 μm ablation at a fluence of 240 J/cm^2). Debris was pooled by washing it off the windows with d_6-DMSO. During the long-term process of debris collection, we often used one fresh cornea for several (maximum 4) CaF_2 windows. Purified collagen in d_6-DMSO was used as a control. Before ^{13}C-NMR measurements, both control and debris samples were equilibrated for 24 h in DMSO

at room temperature. This largely removed the NaCl used in collagen purification. To avoid the possibility of additional thermal chemistry, heat treatment was not used to increase sample solubility.

^{13}C-NMR spectra were recorded of natural-isotope-abundance samples at 22°C in 5-mm tubes, using a 500 MHz Bruker DRX spectrometer (operating at 125 MHz for direct ^{13}C-detection). Chemical shifts were referenced internally to DMSO (39.5 ppm), which also served as the ^{2}H lock solvent. Typical experimental conditions included: a 3° pulse tip angle; 32K data points; a recycle delay of 1.5 seconds; 120K scans; and the presence of broadband proton decoupling during the acquisition period (0.5 s). Measurement of each ^{13}C-NMR spectrum took ~ 66 h of instrument time.

SDS-polyacrylamide gel electrophoresis

For each wavelength, we pooled debris from 30 windows. Debris was pooled by washing it off the windows with distilled water. After the water was removed by vacuum-drying, the 30 windows yielded ~ 300 μg of dried debris. An unexposed cornea was minced and dried for use as a control sample (1 mg dry material). The barely soluble proteins were then extracted from the dried materials using a 5% SDS solution at 4°C. Initially, 200 μl of the SDS solution was added for each 300 μg of dried sample. The samples were mixed and then centrifuged. If centrifugation yielded less than ~ 50 μl of supernatant, more SDS solution was added, the pellet was resuspended and the sample centrifuged again. Approximately 10% of each supernatant was used per gel lane. Due to variations in solubility among the samples (solubility decreased from 6.45-μm debris to 2.77-μm debris to minced corneas), it was difficult to accurately load the same amount of material in each gel lane. Electrophoretic separation was carried out with a 5% stacking gel and 12% separating gel. After electrophoresis, the separating gel was stained with 0.1% Coomassie Blue, and destained in 7% acetic acid. Gels were documented with a digital camera.

RESULTS

To avoid confusing laser wavelengths with references to spectral features, we will make an artificial distinction in units: cm^{-1} for FTIR and Raman spectral features; and μm for laser wavelengths. Of course, 2.77 and 6.45 μm are equivalent to 3610 and 1550 cm^{-1}, respectively.

FTIR spectroscopy

As shown in Fig. 1 *A*, FTIR spectra of the nonvolatile ablation debris and of unexposed corneas are all very similar. The dominant features of each spectrum correspond to the vibrational modes of dehydrated collagen. Of particular interest are the CH_2 and CH_3 stretch vibrations (~ 2900 cm^{-1}), as well as the amide I (~ 1653 cm^{-1}) and amide II (~ 1539 cm^{-1}) vibrations of the peptide backbone. Note that these spectra were normalized by the amide I peak. Before normalization, the amide I absorptions ranged from 0.05 to 0.15. For each exposure condition (including the control), spectra from five different CaF_2 window samples are presented.

Small differences become evident upon a closer comparison. These differences are highlighted in the difference spectra (ablation debris minus unexposed cornea) of Fig. 1 *B*. Most importantly, new vibrational bands appear in the high-fluence 6.45-μm debris spectra at 2218 and 2160 cm^{-1}. The 2218 cm^{-1} band is also present in some of the high-fluence 2.77-μm debris spectra, but at a reduced magnitude. These new bands in the debris spectra are evidence of new chemical
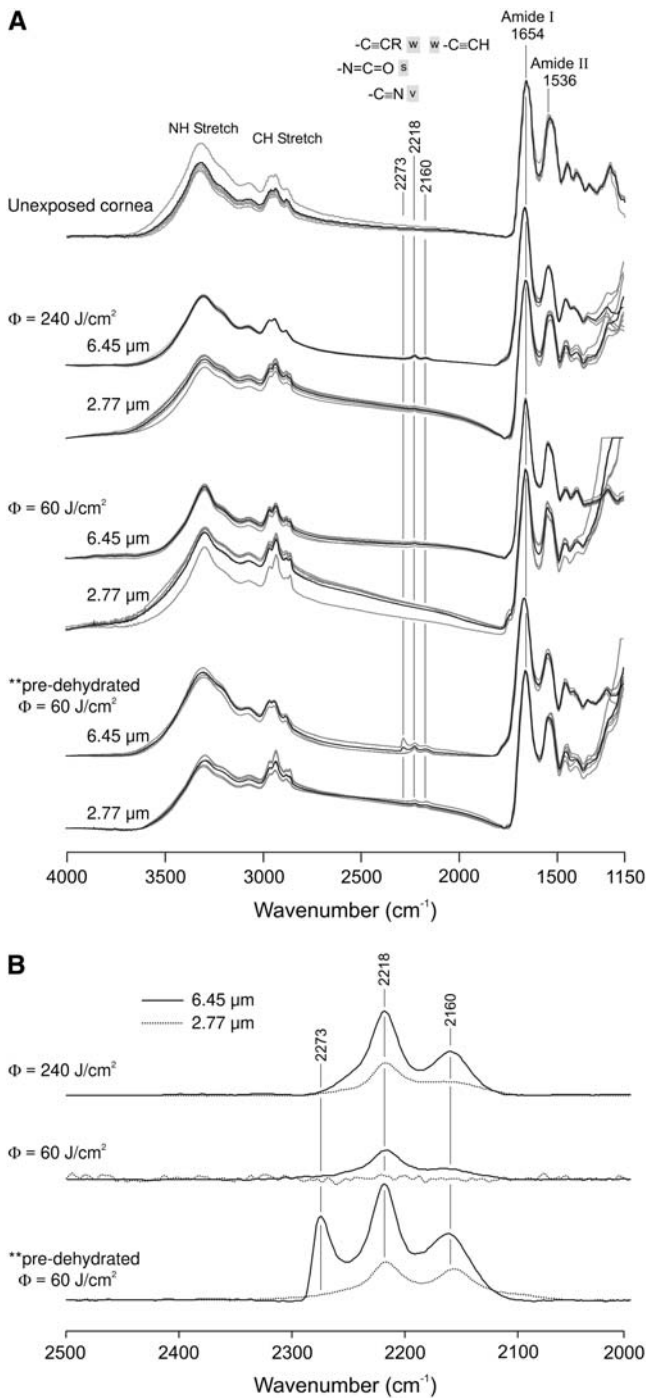
FIGURE 1 FTIR spectra of the debris collected during laser ablation of cornea. (*A*) A set of five independent spectra (*gray*), as well as their average (*black*), are shown for each exposure condition. Spectra from an unexposed cornea are shown for comparison. All samples were vacuum dried on CaF_2 windows. Frequency ranges characteristic of isocyanate, nitrile, and alkyne groups are marked with the gray bars. (*B*) Difference spectra of the average debris spectrum for each condition minus the spectrum of an unexposed cornea. These difference spectra highlight the observed bands of new chemical species.

species. Although FTIR spectra alone cannot definitively identify the new species, the band frequencies lie in a range characteristic of triple-bonds and cumulative double-bonds, e.g., nitrile (-C≡N), isocyanate (-N=C=O), and/or alkyne (-C≡C-) group(s).

Using these amide-I-normalized spectra, we take the baseline-corrected integrated intensity from 2050–2350 cm^{-1} as a measure of new species yield. This yield is strongly dependent on laser wavelength, fluence and the hydration state of the sample. First, the yield is 2–5× larger at 6.45 μm than at 2.77 μm. For the three ablation conditions (240 or 60 J/cm^2 at native hydration, or 60 J/cm^2 for dehydrated corneas), the 6.45-μm yield was 2.4, 4.9, and 2.7-fold larger, respectively. Second, if normal hydration is maintained, then the yield increases with fluence. For 6.45-μm ablation, the yield is 2.8× larger at the higher fluence. For 2.77-μm ablation, it is 5.6× larger at higher fluence. Third, if the fluence is constant, the yield of new species increases when the corneas are allowed to first dehydrate. At 60 J/cm^2 and 6.45 μm, dehydration increases the yield by a factor of 5.2. At 60 J/cm^2 and 2.77 μm, dehydration increases the yield by a factor of 9.4. Part of this increased yield in the low-fluence debris from dehydrated corneas comes from an additional new band at 2273 cm^{-1}. This band is also in the triple-bond spectral range. In summary, FTIR spectra of the ablation debris show the following: a marked wavelength-dependence (differences between the debris and control spectra are always larger for 6.45 μm than for 2.77 μm); a marked fluence-dependence (the differences are reduced, if not eliminated, at lower fluence); and a hydration-dependence (dehydration before ablation leads to much larger spectral differences).

One concern is that the new chemical species could have arisen from post-ablation effects. The spacing between spots was sufficient to minimize inter-spot effects, i.e., exposure of debris already on the window to the pulses used to ablate subsequent spots; however, 5–10 macropulses were typically used at any single ablation spot. Thus, material ejected during the first few pulses at each location was exposed to subsequent FEL macropulses while on, or on the way to, the CaF_2 window surface. To minimize such effects, we also measured FTIR spectra of debris collected with the sample and CaF_2 window tilted 45° with respect to the FEL beam (not shown). This setup does not collect the debris as efficiently, but it does reproduce the spectral changes observed in on-axis collection.

Micro-Raman spectroscopy

We next measured micro-Raman spectra of the debris collected from single macropulse (240 J/cm^2) ablation. Fig. 2 shows light micrographs of the collected debris fields and Raman spectra of individual debris droplets. It is immediately obvious that the 2.77- and 6.45-μm debris fields have very different morphologies: the 6.45-μm debris consists of small, round droplets; whereas the 2.77-μm debris has much
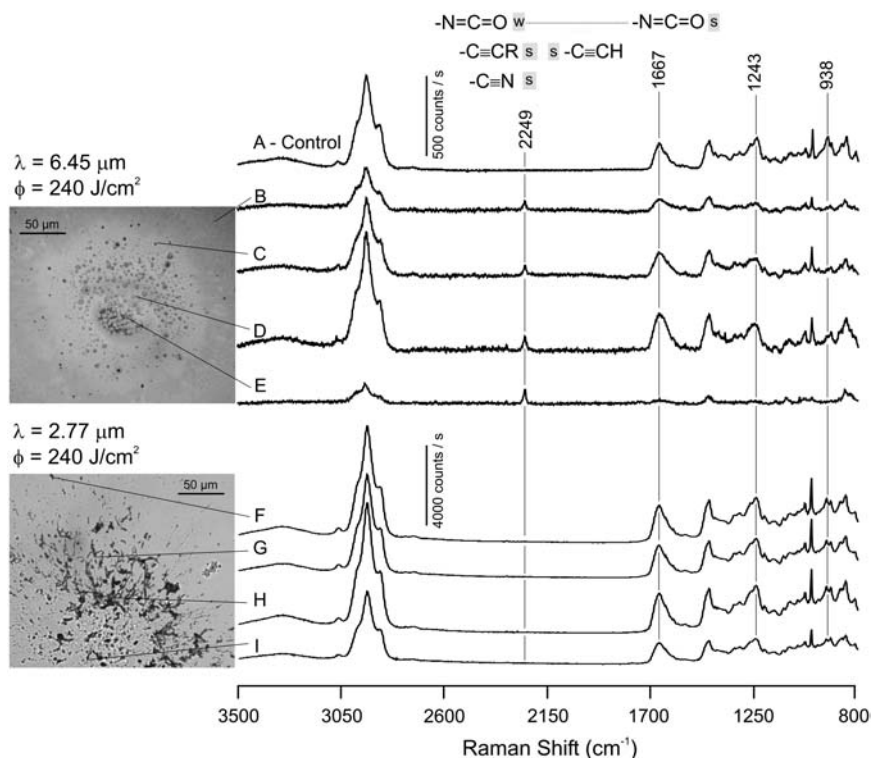
FIGURE 2 Micro-Raman spectra of the debris collected during laser ablation of cornea. Each spectrum was collected from a single dried droplet of debris on a CaF$_2$ window. The droplet corresponding to each spectrum is marked with a thin pointer line. A spectrum from an unexposed cornea is shown for comparison. Frequency ranges characteristic of isocyanate, nitrile, and alkyne groups are marked with the gray bars.

larger, and certainly not round, tissue fragments. These differences are consistent with previous observations (5).

Overall, the Raman spectra of individual droplets and unexposed corneal slices are very similar. The major peaks in each are consistent with reference spectra (8,9), but there are reproducible differences. For ablation at 6.45 μm, but not at 2.77 μm, the Raman spectra again have evidence of new chemical species, in this case a new vibrational band at 2249 cm^{-1}. For some spectra (not shown), this band is broadened toward lower frequencies with an apparent shoulder around 2220 cm^{-1}. Both bands are again in a spectral region characteristic of triple-bonds or cumulative double-bonds.

The droplets corresponding to each spectrum are marked in the insets to Fig. 2. The new 2249 cm^{-1} band appears in all 6.45-μm debris droplets—from the center of the exposed region up to ~240 μm away. The relative intensity of this band (compared to the amide I peak near 1667 cm^{-1}) is approximately the same in most droplets. It is however much larger in the central damaged region (where the center of the ablating beam passed though the window). Nonetheless, these spectra demonstrate that the new chemical species can be generated by exposure to a single macropulse. This further alleviates our concerns about the subsequent exposure of debris already on the window.

^{13}C-NMR spectroscopy

To further investigate the nature of the changes taking place during ablation, we measured natural-abundance ^{13}C-NMR

spectra of the DMSO-solubilized debris. To collect sufficient material for this analysis, we pooled debris from over 200 windows. We chose d$_6$-DMSO over H$_2$O as the solvent for two reasons. First, the debris appears to have a better solubility in DMSO. Second, and more important, the suspected nitrile, isocyanate, and /or alkyne functional group(s) are not as reactive toward DMSO as H$_2$O.

A comparison of ^{13}C-NMR spectra from purified corneal collagen and the high-fluence 6.45-μm debris is shown in Fig. 3. The control spectrum of purified corneal collagen agrees very well with previously reported ^{13}C-NMR spectra of collagens (10–13). This agreement is, in general, extended to the debris spectrum. Of particular note are two signatures typically assigned to triple-helical collagen: the carbonyl resonance is split into three bands at 168, 170, and 173 ppm (10,13); and the Ala C$_\beta$ resonance has a chemical shift of 18 ppm (11,14). The largest spectral differences are new resonances in the 6.45-μm debris at 116, 76, and 73 ppm. These bands are further evidence of new chemical species produced during ablation. The 116 ppm resonance lies in a chemical shift range indicative of a nitrile carbon; and the 76 and 73 ppm bands are in the range expected for alkyne carbons (15). Note that we have not been able to measure ^{13}C-NMR spectra from the 2.77-μm debris because even in DMSO this debris has very low solubility.

More subtle differences between the control and debris spectra are observed in the relative intensities of the resonances at 70 and 68 ppm which have been previously assigned to *trans*- and *cis*-Hyp C$_\gamma$, respectively (16). In the
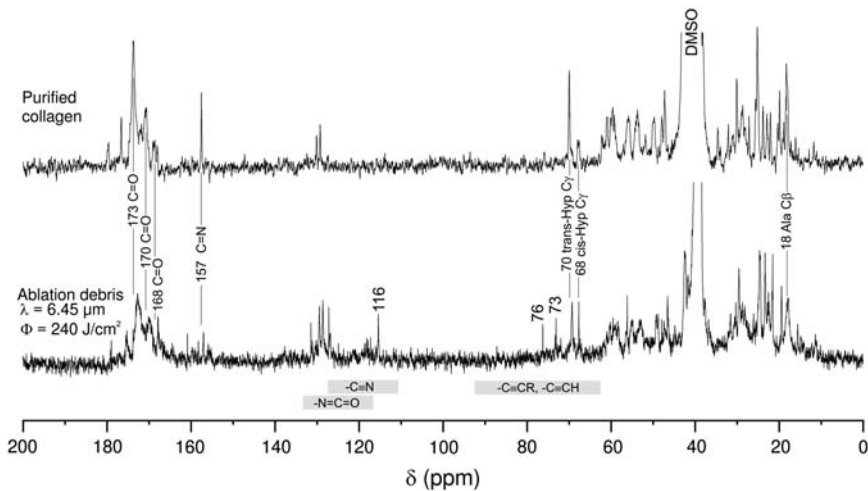
FIGURE 3 ^{13}C-NMR spectra of purified collagen and the debris from high-fluence ablation of cornea at 6.45 μm. The chemical shift ranges characteristic of isocyanate, nitrile, and alkyne groups are marked with the gray bars.

purified collagen spectrum, the relative intensities are ~1:4 (*cis*:*trans*), but this ratio increases to ~1:1 in the 6.45-μm debris, indicating an ablation-associated *trans*-to-*cis* isomerization of hydroxyproline residues. Interestingly, *cis*-Hyp is not normally compatible with native triple-helix structure. Additional studies will be necessary to determine exactly how the secondary and tertiary structure of collagen changes during the ablation process.

SDS-PAGE analysis

We next conducted an electrophoretic analysis of the ablation debris to evaluate the degree of ablation-induced bond breakage. The major organic component in cornea consists of insoluble proteins: collagen, proteoglycans, glycoproteins, and keratins. Analysis of these insoluble proteins usually involves (limited) enzymatic digestion to increase their solubility. However, ablation-induced bond breakage could be masked by such digestion. In lieu of digestion, we used high concentration (5%) SDS extracts of the debris. Similar extracts from minced corneas were used as control. Similar SDS-extraction procedures have previously proven useful in the analysis of insoluble proteins (17,18). An SDS-PAGE gel of the extracts is shown in Fig. 4.

The second lane in Fig. 4 is an extract from minced native corneas. The upper end of this lane contains several bands from corneal collagen: two α-forms, i.e., monomers, near 100 kDa; β-forms, or dimers of collagen molecules, near 200 kDa; and a dense region of γ-collagen (trimers) and higher aggregates above 300 kDa. The highest molecular weight region also likely contains some proteoglycan species (6). There are also two lower molecular weight proteins near 54 and 11 kDa. These are soluble proteins similar to BCP 54 and BCP 11/24 from bovine cornea (19,20). The relative concentrations of these proteins are different in this SDS extract when compared to limited enzymatic digestion of cornea. However, the pattern is reproducible and suitable for analyzing proteins in the ablation debris.

The third and fourth lanes in Fig. 4 are extracts from the high-fluence debris at 6.45 and 2.77 μm, respectively. One cannot directly compare the band intensities between lanes because the solubility was not constant; the 6.45-μm debris was more soluble than the 2.77-μm debris, which was in turn more soluble than the minced corneas. Nonetheless, the relative band intensities within each lane are clearly quite different. For minced cornea, the very large aggregates (>300 kDa) stain much more densely than the α- and β-collagens, and there is no obvious staining of very small proteins below BCP 11/24. In contrast, the 6.45-μm debris has no obvious staining of the very large aggregates nor of α- and β-collagens, yet there is a broad band of very small proteins
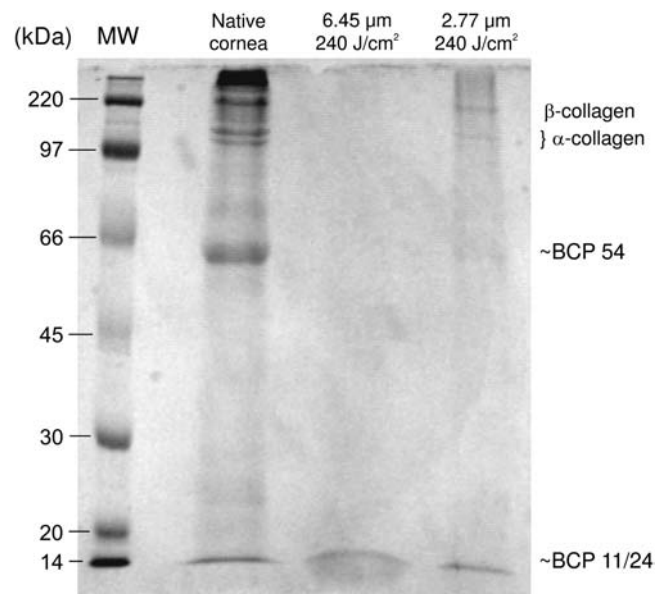

FIGURE 4 Representative SDS-PAGE gel comparing detergent extracts of native cornea to the ablation debris collected at high fluence and either 6.45 or 2.77 μm. Identifiable bands are denoted down the right-hand side. The leftmost lane contains molecular weight markers.

below BCP 11/24. The 2.77-μm debris is more similar to the minced cornea, but staining of the high molecular weight aggregates is not as intense relative to the α- and β-collagens. As in the minced cornea, there is no obvious staining of very small proteins below BCP 11/24. In summary, the 2.77-μm debris appears to have more monomers and dimers relative to larger aggregates, which suggests a loss of covalent cross-linking. The 6.45-μm debris has more small protein fragments relative to the monomers, dimers and aggregates, which suggests not only a loss of cross-linking, but also scission of the protein backbones.

DISCUSSION

The dominant contribution to the tensile strength of soft biological tissues comes from collagen fibers. During laser ablation of soft tissue, the structural integrity of these collagen fibers must fail. In this report, we examine the molecular nature of this failure and the hypothesis that protein structural failure can be influenced by laser wavelength in the mid-IR. Compiling all the spectroscopic and electrophoretic evidence, we come to the following three conclusions. First, at very high fluence (240 J/cm^2) and a wavelength of 6.45 μm, the individual collagen monomers are fragmented. Second, we detect two new chemical species in the debris (nitriles and alkynes) that indicate this fragmentation occurs by scission of the protein backbone at N-alkylamide bonds. Third, both laser wavelength and fluence can alter the molecular nature of this structural failure. The evidence for each of the above claims is compiled and critiqued below.

Collagen monomers are fragmented

The main evidence for protein fragmentation comes from the SDS-PAGE results. For high-fluence 6.45-μm ablation debris, the only visibly stained bands in the SDS extracts were the soluble protein similar to BCP 11/24 and a range of lower molecular weight (MW) fragments. No staining is evident in the higher MW region where one would expect collagen monomers, dimers and aggregates. If more of this debris extract is loaded on the gel, the low MW bands stain much more intensely, but the collagen bands remain faint at best. In contrast, no other debris or control preparation showed any evidence of small fragments below BCP 11/24, even when the collagen bands were very densely stained. We have noted the difficulty in loading the same amount of protein in each lane due to large differences in solubility; however, the increased solubility of the 6.45-μm debris provides indirect confirmation that this debris is broken into smaller fragments.

One would not expect to see direct evidence of this fragmentation in the FTIR, Raman, and NMR spectra. At 6.45-μm, the smallest fragments observed from electrophoresis are on the order of 10 kDa. Such fragments could be generated by breaking only ~1% of the backbone bonds per

collagen molecule. In the spectra we have collected, a 1% decrease in relative intensity is not reliably detectable. Nevertheless, indirect evidence is observed in these spectra via the detection of new chemical species (see below).

Fragmentation occurs via scission at N-alkylamide bonds

The first step toward establishing the site of fragmentation is to identify the new species formed during ablation. These species appear under the same conditions that lead to fragmentation; and just as importantly, they are greatly reduced or eliminated under conditions that do not. For high-fluence 6.45-μm ablation of fully hydrated corneas, we have observed the following spectroscopic signatures of these species: three new ^{13}C-NMR resonances at 116, 76, and 73 ppm; and three new vibrational modes at 2249, 2218, and 2160 cm^{-1} each with very different IR and Raman activities. The 2249-cm^{-1} mode is very Raman active with no detectable IR activity. The 2218-cm^{-1} mode has both Raman and IR activity; and the 2160-cm^{-1} mode is barely discernable in the IR and not observed in Raman spectra. Nonetheless, the new vibrational bands all lie within the triple-bond or cumulative double-bond region. Since the peptide backbone is composed solely of H, C, N, and O atoms, there are three classes of molecular species consistent with the vibrational bands: nitriles, including cyanates and cyanamides (-C≡N); isocyanates (-N=C=O); and either mono- or di-substituted alkynes (-C≡CH, -C≡C-).

The evidence for the formation of nitrile species is by far the strongest. The CN stretching mode of nitrile groups is typically found between 2200–2260 cm^{-1} with substantial IR and Raman activity (21–24). The CC stretching mode of di-substituted alkynes overlaps this range, but such modes should have very strong Raman activity and weak IR activity (23). Thus, we assign the 2218 cm^{-1} vibrational mode to a generalized nitrile species. Within the nitrile class, the 2218 cm^{-1} band is most consistent with the ranges established for cyanamides and conjugated nitriles (23,24). However, the stretching frequency of cyanates or aliphatic nitriles might be pushed into this region by hydrogen bonding in the protein debris. Identification of the specific nitrile species produced will require additional model compound studies. Further evidence for nitrile species is found in the ^{13}C-NMR spectra where nitriles typically have a resonance between 112–126 ppm (15). Few other groups have resonances that overlap this range, making it highly diagnostic for nitriles. Thus, we also assign the 116 ppm resonance to a nitrile species.

Evidence for the formation of alkynes is not as definitive, but is still quite strong. As noted above, the CC stretch of alkynes is weak in the IR, but very strong in Raman spectra. All of the other groups under consideration have much more intense IR activity in the triple-bond region. The typical ranges of alkyne CC stretches are 2100-2150 cm^{-1} for mono-substituted and 2190-2260 cm^{-1} for di-substituted species (23). Thus, we assign the new 2249 cm^{-1} mode to a

di-substituted alkyne. This assignment is a bit less definitive because di-substituted alkynes often have a Fermi resonance that leads to two Raman bands in this region (23). For the single 2249 cm^{-1} band to represent a di-substituted alkyne, the Fermi resonance must somehow be suppressed. The ^{13}C-NMR spectra are also consistent with the formation of alkynes, which typically have a pair of ^{13}C-resonances between 65–90 ppm (15). Unfortunately, many other groups also yield ^{13}C-resonances in this region. Thus, we assign the 76 and 73 ppm resonances to an alkyne species, but do so tentatively. Although the alcohols and ethers of carbohydrate moieties in the cornea's proteoglycans are possible alternative sources, these carbohydrates should also have a prominent resonance around 100 ppm that we do not observe (25,26).

These assignments leave two spectroscopic signatures unaccounted for: a 2160 cm^{-1} IR band; and a 2273 cm^{-1} IR band that is only observed during ablation of severely dehydrated corneas. The 2160 cm^{-1} band may be a second band arising from Fermi resonance within the nitrile species discussed above. A weaker, lower frequency IR band often accompanies the main CN stretch of nitrile species (e.g., 27). Consistent with this interpretation is the fact that we do not have any unassigned ^{13}C-NMR resonances. Alternatively, the 2160 cm^{-1} band is on the upper edge of the range expected for monosubstituted alkynes (23). Monosubstitution of alkynes does increase their IR activity and decrease their Raman activity. However, if the 2160 cm^{-1} band does represent a monosubstituted alkyne, then this group must be formed in much lower abundance than the disubstituted alkyne discussed above. As for the 2273 cm^{-1} band, it is most consistent with an isocyanate group (-N=C=O). Isocyanates have a strong IR band (and a weak or absent Raman band) between 2250–2300 cm^{-1} (23). We do not have supporting Raman and ^{13}C-NMR evidence for this assignment. We have attempted to measure Raman spectra from the ablation of severely dehydrated corneas, but the signal/noise ratio is very poor due to immense background fluorescence (probably from char in the debris).

Returning to the two species for which we do have strong evidence, the formation of nitrile and disubstituted alkyne groups is most readily explained by the scission of N-alkylamide bonds. Such scissions would yield a terminal amide radical on one side, which upon dehydration would generate a terminal nitrile. The other side of these scissions would yield a ketone radical. A similar loss of a water molecule from the ketone could then yield a disubstituted alkyne. Note that a monosubstituted alkyne would form if the amino acid at the scission site were a glycine (~33% of the residues in collagen). A similar scission of the weakest N-alkylamide bond has been well accepted for the appearance of nitrile groups in the thermal degradation of aliphatic nylons (28 and references therein). This one scission reaction plausibly accounts for the protein fragmentation seen via electrophoresis and both of the new species seen in our spectroscopic analysis.

Laser wavelength and fluence alter the molecular nature of collagen structural failure

For the set of laser ablation experiments presented here, we used two matched wavelengths, i.e., our sample tissue (porcine cornea) had the same absorption coefficient at both 2.77 and 6.45 μm. Nonetheless, the biochemical changes in the debris were wavelength- and fluence-dependent. Two clear examples of the wavelength-dependence are the greater accumulation of new nitrile species and the greater protein fragmentation in the 6.45-μm debris. A clear example of the fluence-dependence is the greater accumulation of nitrile species at higher fluence (240 compared to 60 J/cm^2). Although the dependencies observed here are consistent with those observed for collateral damage, further studies will be necessary to establish a tighter correlation. A major remaining challenge is to establish whether the collagen fragmentation observed here causes a loss of higher-order (i.e., tissue-level) structural integrity; and if so, does this ultimately lead to a reduction in collateral damage.

One potentially trivial source for the wavelength-dependence is that debris ejected during the first few macropulses, which is dehydrated and thus has a much lower 2.77-μm absorption coefficient, is subsequently exposed to several additional pulses. Two results suggest this is an unlikely source. First, FTIR bands corresponding to the new species are also observed in 6.45-μm debris collected off-axis. Second, micro-Raman spectra of the 6.45-μm debris have the same new band (2249 cm^{-1}) for multiple-pulse and single-pulse ablation. Furthermore, this band is clearly observable in debris droplets that impacted the window at points well outside the irradiated area.

A second potential, but also unlikely, source is that the chosen wavelengths were not dynamically matched. These two wavelengths are matched on the basis of linear spectroscopy at room temperature; however, absorption in the 3-μm region is notoriously temperature dependent (29). As the temperature rises, the OH stretch manifold of water decreases in intensity and shifts to higher frequency. Fortunately, 2.77 μm is on the blue side of the OH stretch band where the intensity decrease and band shift counteract one another. The result is a 2.77-μm absorption coefficient with a weak temperature dependence similar to that noted for Er:YSSG (2.79 μm) laser ablation (30). Temperature-dependent band shifts are also quite weak in the 6–7 μm region. Thus, up to the onset of vaporization, the dynamic absorption coefficients at 2.77 and 6.45 μm should be reasonably well matched.

A third, and more likely, source is that each wavelength targets a different chromophore: predominantly water at 2.77 μm and protein at 6.45 μm. Whether this targeting affects collagen scission and the ablation process via thermal, mechanical, or chemical means is still an open question. As shown in Fig. 5, FTIR spectra of corneal samples heated to 200–500°C do show a new band around 2218 cm^{-1}, but it is always accompanied by extensive changes in the amide I, II,
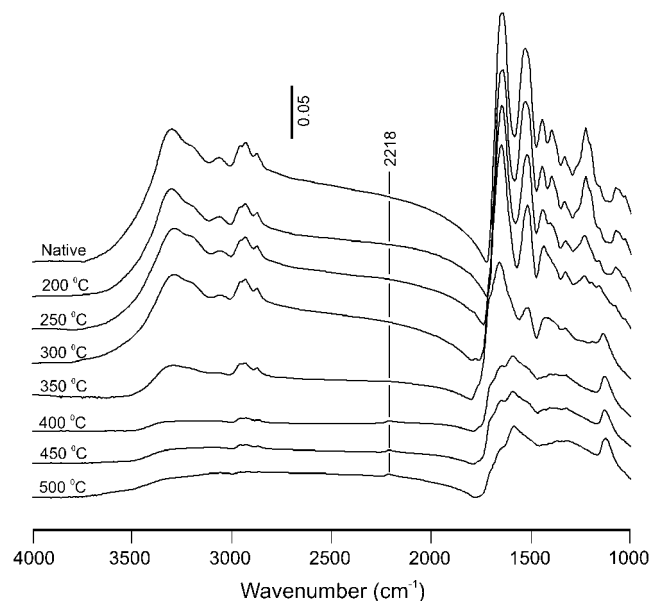
FIGURE 5 FTIR absorbance spectra of thin slices of dehydrated cornea heated in air to temperatures between 200–500°C for 2 min. Although a 2218 cm^{-1} band does grow in as the temperature is increased above 350°C, it is accompanied by numerous spectral changes in the amide I, II, and III regions (1000–1700 cm^{-1}). The scale bar applies to absorbance units for all spectra.

and III regions that are not present in our debris spectra. Thus, an equilibrium thermal process is unlikely. Previous models have favored a nonequilibrium photothermal mechanism where direct absorption by tissue proteins leads to greatly elevated protein temperatures, as compared to the surrounding water (31,32). These higher temperatures then lead to a loss of protein structural integrity through a transition that is thermally-activated, but otherwise ill-defined. The results presented here suggest a candidate for the relevant structural failure—scission of N-alkylamide bonds—but this hypothesis must be further tested. Additional evidence in support of chromophore-targeting is that similar yields of new species are observed when corneas are ablated at 6.1 μm (not shown). Protein absorption is nearly the same at 6.1 and 6.45 μm, but the energy is absorbed by a different protein vibrational mode. To complicate matters, there is also stronger absorption by water at 6.1 μm. Nonetheless, the ability of both wavelengths to fragment collagen suggests a lack of mode specificity. Both wavelengths also ablate tissue well, and in some cases, 6.1-μm ablation is superior to 6.45 μm (33). One certain future direction is a careful examination of laser-induced collagen scission across the 2–9-μm tuning range of the Vanderbilt FEL.

This example shows how the molecular view expounded here, and the spectroscopic markers of scission, will be important tools for addressing a number of mechanistic questions. As another example, measurements of the scission yield as a function of FEL micropulse structure are planned to eluci-

date the potential role of nonlinear (multiphoton) processes. Additional measurements of scission yield under inert atmospheres will address the potential role of molecular oxygen—all experiments to date have been performed in air. The results presented here are a first step. They enable future experiments that will help unravel the physical mechanism that minimizes collateral damage in the 6–7-μm wavelength range.

REFERENCES

1. Vogel, A., and V. Venugopalan. 2003. Mechanisms of pulsed laser ablation of biological tissues. *Chem. Rev.* 103:577–644.

2. Wolbarsht, M. L. 1984 Laser surgery—CO2 or HF. *IEEE J. Quantum Electron.* QE-20:1427–1432.

3. Edwards, G., R. Logan, M. Copeland, L. Reinisch, J. Davidson, B. Johnson, R. Maciunas, M. Mendenhall, R. Ossoff, J. Tribble, J. Werkhaven, and D. O'Day. 1994. Tissue ablation by a free-electron laser tuned to the amide-II band. *Nature.* 371:416–419.

4. Kahle, G., H. Stadter, T. Seiler, and J. Wollensak. 1992. Gas-chromatographic and mass spectroscopic analysis of excimer and erbium - yttrium-aluminum-garnet laser-ablated human cornea. *Invest. Ophthalmol. Vis. Sci.* 33:2180–2184.

5. Auerhammer, J. M., R. Walker, A. F. G. van der Meer, and B. Jean. 1999. Dynamic behavior of photoablation products of corneal tissue in the mid-IR: a study with FELIX. *Appl. Phys. B.* 68:111–119.

6. Tseng, S. C. G., D. Smuckler, and R. Stern. 1982. Comparison of collagen types in adult and fetal bovine corneas. *J. Biol. Chem.* 257:2627–2633.

7. Madey, J. M. J. 1971. Stimulated emission of Bremsstrahlung in a periodic magnetic field. *J. Appl. Phys.* 42:1906–1930.

8. Mizuno, A., M. Tsuji, K. Fujii, K. Kawauchi, and Y. Ozaki. 1994. Near-infrared Fourier-transform Raman-spectroscopic study of cornea and sclera. *Jpn. J. Ophthalmol.* 38:44–48.

9. Frushour, B. G., and J. L. Koenig. 1975. Raman-scattering of collagen, gelatin, and elastin. *Biopolymers.* 14:379–391.

10. Saito, H., R. Tabeta, A. Shoji, T. Ozaki, I. Ando, and T. Miyata. 1984. A high-resolution C-13-NMR study of collagenlike polypeptides and collagen fibrils in solid-state studied by the cross-polarization magic angle-spinning method—manifestation of conformation-dependent C-13 chemical-shifts and application to conformational characterization. *Biopolymers.* 23:2279–2297.

11. Fujisawa, R., and Y. Kuboki. 1990. High-resolution solid-state nuclear-magnetic-resonance spectra of dentin collagen. *Biochem. Biophys. Res. Commun.* 167:761–766.

12. Reichert, D., O. Pascui, E. R. de Azevedo, T. J. Bonagamba, K. Arnold, and D. Huster. 2004. A solid-state NMR study of the fast and slow dynamics of collagen fibrils at varying hydration levels. *Magn. Reson. Chem.* 42:276–284.

13. Saito, H., and M. Yokoi. 1992. A C-13 NMR-study on collagens in the solid-state—hydration dehydration-induced conformational change of collagen and detection of internal motions. *J. Biochem. (Tokyo).* 111:376–382.

14. Saito, H., R. Tabeta, T. Asakura, Y. Iwanaga, A. Shoji, T. Ozaki, and I. Ando. 1984. High-resolution C-13 NMR-study of silk fibroin in the solid-state by the cross-polarization magic angle spinning method—conformational characterization of silk-I and silk-II type forms of Bombyx-Mori fibroin by the conformation-dependent C-13 chemical-shifts. *Macromolecules.* 17:1405–1412.

15. Levy, G. C., R. L. Lichter, and G. L. Nelson. 1980. Carbon-13 Nuclear Magnetic Resonance Spectroscopy. John Wiley & Sons, New York.

16. Sarkar, S. K., P. E. Young, C. E. Sullivan, and D. A. Torchia. 1984. Detection of *cis* and *trans* X-pro peptide-bonds in proteins by C-13 NMR—application to collagen. *Proc. Natl. Acad. Sci. USA.* 81:4800–4803.

17. Ishii, K., N. Tsutsui, T. Watanabe, T. Yanagisawa, and H. Nagasawa. 1998. Solubilization and chemical characterization of an insoluble matrix protein in the gastroliths of a crayfish, *Procambarus clarkii. Biosci. Biotechnol. Biochem.* 62:291–296.

18. Moore, P. N., S. Puvvada, and D. Blankschtein. 2003. Role of the surfactant polar head structure in protein-surfactant complexation: zein protein solubilization by SDS and by SDS/C12En surfactant solutions. *Langmuir.* 19:1009–1016.

19. Cooper, D. L., E. W. Baptist, J. Enghild, H. Lee, N. Isola, and G. K. Klintworth. 1990. Partial amino-acid-sequence determination of bovine corneal protein 54-K (BCP-54). *Curr. Eye Res.* 9:781–786.

20. Bakker, C., S. Pasmans, C. Verhagen, M. Vanharen, R. Vandergaag, and R. Hoekzema. 1992. Characterization of soluble protein-BCP-11/24 from bovine corneal epithelium, different from the principal soluble protein-BCP-54. *Exp. Eye Res.* 54:201–209.

21. Jesson, J. P., and H. W. Thompson. 1962. Intensities of Raman vibrational bands. I. *Proceedings of the Royal Society of London Series A-Mathematical and Physical Sciences* 268:68–78.

22. Jesson, J. P., and H. W. Thompson. 1958. Vibrational band intensities of the CN group in aliphatic nitriles. *Spectrochim. Acta.* 13:217–222.

23. Socrates, G. 2001. *Infrared and Raman Characteristic Group Frequencies: Tables and Charts.* John Wiley & Sons, New York.

24. Kitson, R. E., and N. E. Griffith. 1952. Infrared absorption band due to nitrile stretching vibration. *Anal. Chem.* 24:334–337.

25. Huckerby, T. N., and R. M. Lauder. 2000. Keratan sulfates from bovine tracheal cartilage—structural studies of intact polymer chains using H-1 and C-13 NMR spectroscopy. *Eur. J. Biochem.* 267:3360–3369.

26. Melo, M. R. S., J. P. A. Feitosa, A. L. P. Freitas, and R. C. M. de Paula. 2002. Isolation and characterization of soluble sulfated polysaccharide from the red seaweed *Gracilaria* cornea. *Carbohydr. Polym.* 49:491–498.

27. Compton, D. A. C., W. F. Murphy, and H. H. Mantsch. 1981. Spectroscopic and thermodynamic studies of unsaturated nitrile compounds 2—the infrared and Raman spectra, normal coordinate analysis and values for the ideal gas thermodynamic functions of 3-methyl-2-butenenitrile. *J. of Raman Spectrosc.* 11:349–355.

28. Levchik, S. V., E. D. Weil, and M. Lewin. 1999. Thermal decomposition of aliphatic nylons. *Polym. Int.* 48:532–557.

29. Shori, R. K., A. A. Walston, O. M. Stafsudd, D. Fried, and J. T. Walsh. 2001. Quantification and modeling of the dynamic changes in the absorption coefficient of water at lambda = 2.94 microns. *IEEE Journal of Selected Topics in Quantum Electronics.* 7:959–970.

30. Cummings, J. P., and J. T. Walsh. 1993. Erbium laser ablation—the effect of dynamic optical-properties. *Appl. Phys. Lett.* 62:1988–1990.

31. Hutson, M. S., S. A. Hauger, and G. Edwards. 2002. Thermal diffusion and chemical kinetics in laminar biomaterial due to heating by a free-electron laser. *Phys. Rev. E.* 65:061906.

32. Edwards, G. S., and M. S. Hutson. 2003. Advantage of the Mark-III FEL for biophysical research and biomedical applications. *J. Synchrotron Radiat.* 10:354–357.

33. Youn, J.-I., P. Sweet, G. M. Peavy, and V. Venugopalan. 2006. Mid-IR laser ablation of articular and fibro-cartilage: a wavelength dependence study of thermal injury and crater morphology. *Lasers Surg. Med.* 38:218–228.